Spatially resolved photochemistry impacts emissions estimates in fresh wildfire plumes

Brett B Palm[1], Qiaoyun Peng[2], Samuel R Hall[3], Kirk Ullmann[3], Teresa L Campos[3], Andrew J. Weinheimer[3], Denise D. Montzka[3], Geoffrey Stuart Tyndall[3], Wade Permar[4], Lu Hu[4], Frank Flocke[3], Emily V Fischer[5], and Joel A Thornton[6]

[1]National Center for Atmospheric Research
[2]Department of Atmospheric Sciences, University of Washington
[3]National Center for Atmospheric Research (UCAR)
[4]University of Montana
[5]Colorado State University
[6]University of Washington

November 24, 2022

Abstract

Wildfire emissions affect downwind air quality and human health. Predictions of these impacts using models are limited by uncertainties in emissions and chemical evolution of smoke plumes. Using high-time-resolution aircraft measurements, we illustrate spatial variations that can exist horizontally and vertically within a plume due to differences in the photochemical environment. Dilution-corrected mixing ratio gradients were observed for reactive compounds and their oxidation products, such as nitrous acid, catechol, and ozone, likely due to faster photochemistry in optically-thinner plume edges relative to darker plume cores. Mixing ratio gradients in midday plumes, driven by j_{HONO} gradients, are often steepest in the freshest transects, and become flatter with chemical aging. Gradients in plumes emitted close to sunset are characterized by titration of O_3 in the plume and little to no gradient formation. We show how gradients can lead to underestimated emission ratios for reactive compounds and overestimated emission ratios for oxidation products.

Hosted file

`essoar.10507729.1.docx` available at https://authorea.com/users/547038/articles/602621-spatially-resolved-photochemistry-impacts-emissions-estimates-in-fresh-wildfire-plumes

Brett B. Palm[1,*,#], Qiaoyun Peng[1], Samuel R. Hall[2], Kirk Ullmann[2], Teresa L. Campos[2], Andrew Weinheimer[2], Deedee Montzka[2], Geoffrey Tyndall[2], Wade Permar[3], Lu Hu[3], Frank Flocke[2], Emily V. Fischer[4], Joel A. Thornton[1]

[1]Department of Atmospheric Sciences, University of Washington, Seattle, WA, USA 98195

[2]Atmospheric Chemistry Observations and Modeling Laboratory, National Center for Atmospheric Research, Boulder, CO, USA 80301

[3]Department of Chemistry and Biochemistry, University of Montana, Missoula, MT, USA 59812

[4]Department of Atmospheric Science, Colorado State University, Fort Collins, CO, USA 80523

[@]Now at: Atmospheric Chemistry Observations and Modeling Laboratory, National Center for Atmospheric Research, Boulder, CO, USA 80301

[#]Corresponding author: Brett B. Palm (bbpalm@ucar.edu)

Key Points:

- Spatial gradients are observed in dilution-corrected mixing ratios of nitrous acid, ozone, and reactive organics in fresh wildfire plumes
- Gradients evolve with time of day, as intensity of chemical aging varies relative to plume transport and mixing
- Gradients should be considered when comparing plume models with measurements and estimating fire emissions from in situ observations

Abstract

Wildfire emissions affect downwind air quality and human health. Predictions of these impacts using models are limited by uncertainties in emissions and chemical evolution of smoke plumes. Using high-time-resolution aircraft measurements, we illustrate spatial variations that can exist horizontally and vertically within a plume due to differences in the photochemical environment. Dilution-corrected mixing ratio gradients were observed for reactive compounds and their oxidation products, such as nitrous acid, catechol, and ozone, likely due to faster photochemistry in optically-thinner plume edges relative to darker plume cores. Mixing ratio gradients in midday plumes, driven by j_{HONO} gradients, are often steepest in the freshest transects, and become flatter with chemical aging. Gradients in plumes emitted close to sunset are characterized by titration of O_3 in the plume and little to no gradient formation. We show how gradients can lead to underestimated emission ratios for reactive compounds and overestimated emission ratios for oxidation products.

Plain Language Summary

Wildfire emissions have large impacts on air quality and health in downwind communities. Previous research has shown that chemical reactions in fire plumes

can be remarkably fast, which modifies the impact the smoke has downwind. In this work, we show how this chemistry happens faster on the edges versus the core of plumes emitted during midday. For plumes emitted near or after sunset, oxidation chemistry generally slows and remains nearly uniform across the plume. These variations in plume chemistry will impact how plumes are modeled, and how well we can predict downwind air quality impacts.

1. Introduction

Wildfire emissions are becoming increasingly important drivers of degraded air quality, especially in the Western U.S. (McClure & Jaffe, 2018; O'Dell et al., 2019). Wildfire season is growing longer and fires are growing larger due to several factors, including climate change, a legacy of fire suppression, and an increasing wildland-urban interface (Abatzoglou & Williams, 2016; Balch et al., 2017; Dennison et al., 2014; Higuera et al., 2021; Higuera & Abatzoglou, 2021; Radeloff et al., 2018; Westerling, 2016). A better understanding of the composition and evolution of wildfire emissions is needed to predict the impacts on downwind communities, atmospheric dynamics, and climate.

In aircraft studies of wildfires and other point sources, emissions are typically evaluated by sampling plume composition in horizontal transects of the plume perpendicular to the wind direction, where each transect corresponds to a similar physical plume age. A regional background abundance from outside the plume is subtracted from the average crosswind transect abundance to determine a normalized excess mixing ratio (NEMR) for each transect (e.g., Akagi et al., 2012; Liu et al., 2017; Palm et al., 2020; Yokelson et al., 2009). The NEMR values in the youngest parts of the plume are often used as estimates of the emission ratio (ER), which is meant to represent the relative emission flux of a species from the fire prior to any substantial physical or chemical changes with aging. ERs and related emission factors (EF; emission per mass of fuel burned) are essential components of biomass burning emissions inventories used in air quality and earth system models (e.g., Andreae, 2019; van der Werf et al., 2017; Wiedinmyer et al., 2011; Yokelson et al., 1999).

Spatial variations in plume chemistry can make NEMRs and ERs dependent upon which portion of the crosswind transects are used in the calculation (e.g., entire transect versus plume core), especially for chemically reactive components. Spatial variation in wildfire plume chemistry has only rarely been investigated in detail across plume transects (Garofalo et al., 2019; Hodshire et al., 2021; Juncosa Calahorrano et al., 2021; Peng et al., 2020). Furthermore, vertical gradients in plume chemistry have not been investigated to our knowledge. We use high-time-resolution measurements to investigate horizontal and vertical spatial variation in wildfire plume chemistry. We show that gradients can be anywhere from steep to nonexistent depending on factors such as physical age or time of day at emission and sampling. Impacts on NEMR calculations are investigated for all crosswind transects sampled during a recent flight campaign. This work shows the importance of considering spatial gradients in oxidation chemistry of fresh wildfire plumes.

1. Materials and Methods

   (a) **WE-CAN campaign**

The Western Wildfire Experiment for Cloud Chemistry, Aerosol Absorption, and Nitrogen (WE-CAN) field campaign took place in the Western U.S. from July–September 2018. Measurements were taken using a suite of instruments installed aboard a C-130 aircraft operated by the National Center for Atmospheric Research (NCAR) and the National Science Foundation (NSF). The C-130 sampled nearly two dozen individual wildfire plumes, targeting fresh emissions and aging up to several hours. Special focus is given to measurements from the Taylor Creek Fire and the South Sugarloaf Fire smoke plumes.

1. **Plume measurements**

The main instrument used in this analysis was an iodide-adduct high-resolution time-of-flight mass spectrometer (I^- CIMS), measuring a suite of gas-phase oxidized organic and inorganic compounds. The I^- CIMS operation has been described in detail in Palm et al. (2020). More details of the I^- CIMS and other instruments used in this analysis can be found in Sect. S1. For this analysis, data from all instruments were smoothed by a 5 s average. Plumes were defined as any data where the enhancement of CO above regional background was greater than 250 ppbv.

NEMR values across transects were calculated by taking the ratio of background-subtracted abundances of each compound to background-subtracted CO using 5 s averaged data. See Sect. S1 for more details of background subtraction.

1. Results and Discussion

   (a) Taylor Creek fire: narrow plume with high [HONO]

      i. Gradients in reactive compound NEMRs

Early on 30 July 2018, the Taylor Creek fire in southern Oregon emitted smoke into a smoke-filled boundary layer with other nearby fires. Soon after the research aircraft arrived in the area, the fire intensity and environmental conditions supported the injection of a fresh plume above the boundary layer (3.3–3.7 km above sea level; ASL) in the relatively clean free troposphere (see pictures in Fig. S1). The plume was narrow (~3–5 km across) with a dense core tapering on either side. The plume was first sampled shortly (~10 min) after it was observed to be injecting into the free troposphere, with an estimated physical age of about 21 min after emission. The aircraft was able to continually resample the leading edge of the plume as it aged from 15:45-18:00 local time (LT), providing a near-Lagrangian experiment.

Crosswind gradients in the Taylor Creek plume can be seen in the map of NEMRs in Fig. 1. With the effects of dilution removed by normalizing to excess CO, the strong horizontal crosswind gradients observed for this suite of reactive compounds and oxidation products were a result of variable rates of chemical loss/production across the plume. For the fastest reacting compounds such as

$C_6H_6O_2$ (likely catechol), HONO (nitrous acid), and $C_7H_8O_2$ (likely methyl catechol, shown in Fig. S2), high mixing ratios were observed only in the core of the first several transects closest to the fire. At these locations, the plume core was at its darkest, as confirmed by j_{HONO}. In the earliest two transects, the dilution-corrected production rate of OH from HONO photolysis was faster on the plume edges relative to the core (Fig. S2). However, even on the edges of the first several transects, HONO was substantially photolyzed and compounds such as $C_6H_6O_2$ (lifetime of 33 min at [OH] = 5 x 10^6 molecules cm^{-3}; Olariu et al., 2000) were already mostly reacted away. Slower reacting compounds such as $C_6H_6O_1$ (likely phenol, lifetime of 2.1 h at [OH] = 5 x 10^6 molecules cm^{-3}; Atkinson et al., 1989) were depleted more gradually with downwind transport, and smaller gradients were observed in the crosswind transects. For compounds that were not reactive on this time scale of several hours of downwind transport, gradients were not observed (or expected) in either the crosswind or downwind directions (e.g., HCN shown in Fig. S2).

For compounds produced from oxidation chemistry, reversed gradients were observed where the compounds were enhanced relative to CO on the plume edges versus the core. This group includes organic oxidation products such as $C_3H_4O_3$ (pyruvic acid and other isomers, as an example of a variety of small organic oxidation products) and ozone (O_3), as shown in Fig. 1. A general trend of increasing NEMRs with increasing age downwind was observed for this subset of compounds. In the Taylor Creek plume, near-field O_3 formation was likely influenced by rapid OH chemistry from HONO photolysis during the mid-day sampling. The Taylor Creek plume contained one of the highest measured HONO ERs of any fire during the campaign (Peng et al., 2020).

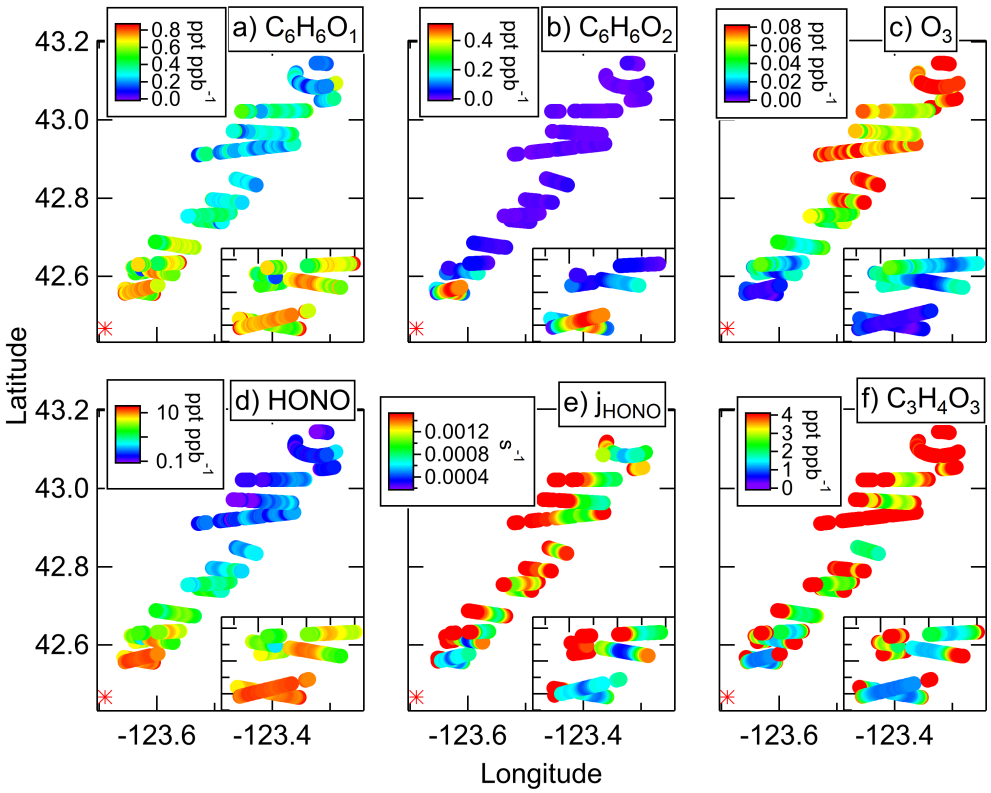

Figure 1. Plume transects of the Taylor Creek fire, showing spatial variations in NEMRs of a) $C_6H_6O_1$, b) $C_6H_6O_2$, c) O_3, d) HONO, e) j_{HONO}, and f) $C_3H_4O_3$. The emission source is marked with an asterisk. Insets show the first five transects in greater detail.

1. Inferred gradients of average OH concentrations in fresh plumes

The gradients observed in the NEMRs of reactive compounds and their oxidation products indicate that the rate of oxidation, and therefore oxidant concentrations, have gradients as well. In the Taylor Creek plume, the large source of OH from HONO photolysis in this relatively bright midday plume meant that OH was likely the dominant oxidant for most compounds. Here, we use the gradients of reactive compounds to infer spatial variations in photochemical aging due to OH oxidation at different locations within the plume.

The average OH radical concentration ($[OH]_{avg}$) experienced by air sampled at any point within the plume since emission can be calculated using Eq. 1, derived from de Gouw et al. (2005) and Roberts et al. (1984). We use the known reaction rates of compounds A and B with OH (k_{OH+A} and k_{OH+B}; see

Table S1 for all rates used), the initial emission ratio of the compounds (at t=0), and the estimated physical time since emission (Δt).

$$[\mathbf{OH}]_{\mathrm{avg}} = \frac{\mathbf{1}}{\mathbf{t}(\mathbf{k_{OH+A}} - \mathbf{k_{OH+B}})} \times \left(\ln\left(\frac{[\mathbf{A}]}{[\mathbf{B}]}\Big|_{\mathbf{t=0}} \right) - \mathbf{ln}\left(\frac{[\mathbf{A}]}{[\mathbf{B}]} \right) \right) \quad (1)$$

This equation can be rearranged to give OH exposure as well (OH_{exp} = $[OH]_{avg}$ x Δt). Equation 1 is valid when OH is the only relevant oxidant for the chosen compounds during Δt. Compounds A and B are chosen such that they react with OH at different rates (and aren't produced as oxidation products) and their ratio of emissions can be estimated. When k_{OH+B} is slow enough that B does not appreciably react during Δt (as is the case for CO), then the sole purpose of compound B is to account for dilution, and Eq. 1 can be simplified to the exponential decay of dilution corrected compound A. The methodology is further described in Sect. S2.

We used $C_6H_6O_2$ and CO as compounds A and B in Eq. 1 to estimate $[OH]_{avg}$ experienced by the plume between emission and the point of sampling across each transect, as shown in Fig. 2. For $C_6H_6O_2$, the nitrate radical (NO_3) is also a relevant oxidant. Since $k_{OH+C6H6O2}$ and $k_{NO3+C6H6O2}$ are nearly equal (1.0 x 10^{-10} and 9.9 x 10^{-11} cm^3 $molecule^{-1}$ s^{-1}, respectively; Olariu et al., 2000, 2004), Eq. 1 provides an estimate of $[OH+NO_3]_{avg}$. Box modeling (Sect. S2) suggests approximately 25% of $C_6H_6O_2$ reacts with NO_3 (and negligible reaction with O_3) in the Taylor Creek Fire plume. Thus, we multiplied the result of Eq. 1 by 0.75 to estimate $[OH]_{avg}$ whenever using $C_6H_6O_2$.

In the several transects closest to the fire with estimated physical age of about 20 min, steep cross-plume gradients were observed for $[OH]_{avg}$ in Fig. 2. On the plume edges where HONO photolysis was faster, we inferred $[OH]_{avg}$ on the order of 1.0 x 10^7 molecules cm^{-3}, while the plume core was much lower at approximately 4 x 10^6 molecules cm^{-3}. In transects further downwind, with physical ages > 45 min, the HONO in the center of the transects had also photolyzed, and the $[OH]_{avg}$ inferred in the plume center was essentially the same as that of the plume edges near 1.0 x 10^7 molecules cm^{-3}. The inferred $[OH]_{avg}$ (and the gradients of other compounds in Fig. 1) was essentially flat across each transect as the plume aged further, decreasing with increasing est. physical age, from 1.0 x 10^7 molec cm^{-3} closer to the fire to 4 x 10^6 molec cm^{-3} after two hours of physical aging. These values are the $[OH]_{avg}$ between emission and sampling, so the actual [OH] in the latter part of this plume was lower. As shown in Fig. S4, OH_{exp} increased rapidly with steep cross-plume gradients over the first several transects, and then increased gradually without cross-plume gradients beyond that age.

The choice of initial ratio of $C_6H_6O_2$ to CO is a potential source of uncertainty. For the calculations above, we used an initial ratio of 1. A sensitivity analysis, discussed in Sect. S3, found that the gradients in $[OH]_{avg}$ were robust for different initial ratios. Analysis of other compound ratios (Sect. S3) illustrates how crosswind $[OH]_{avg}$ gradients are only quantifiable because $C_6H_6O_2$ reacts

fast enough to form measureable crosswind gradients, while compounds such as $C_6H_6O_1$ and C_7H_8 (toluene) are not as useful.

Since the OH source from HONO in this plume was one of the largest measured during WE-CAN, our estimates likely fall near the upper end of [OH] in fresh plumes from fires in this region. Larger and darker plumes, or plumes emitted near or after sunset, may have stronger influence from other oxidants such as NO_3 or O_3. However, crosswind gradients were observed in multiple wildfire plumes sampled during WE-CAN, as shown for the South Sugarloaf fire in the next section and for the broader WE-CAN measurements in Sect. 3.3.

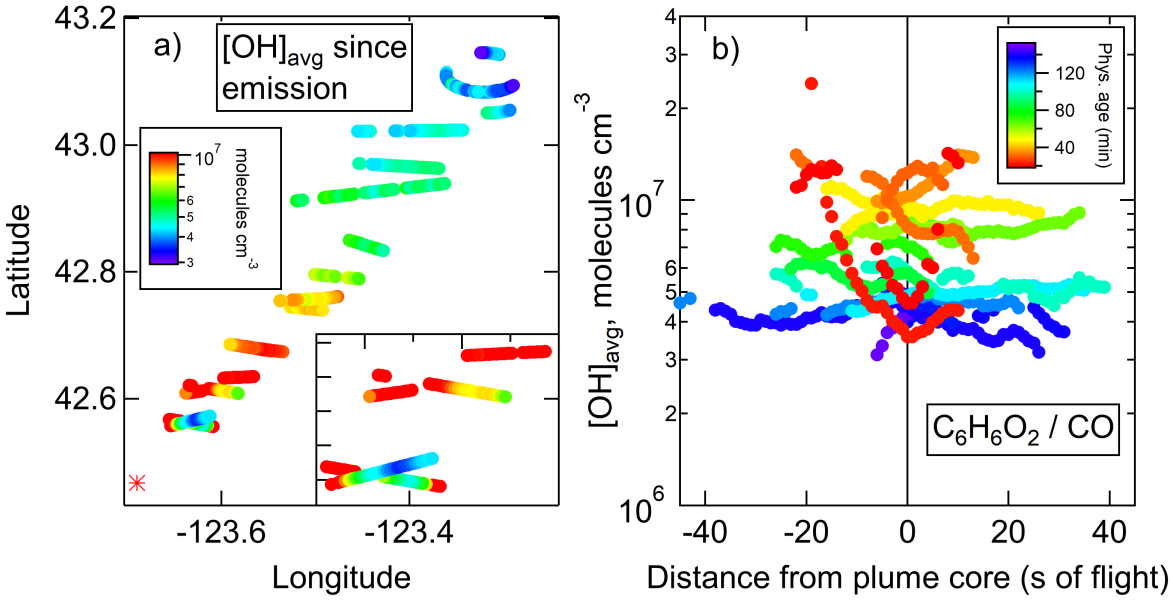

Figure 2. In the Taylor Creek Fire plume, a) $[OH]_{avg}$ between emission source (marked with an asterisk) and each sampled location, and b) $[OH]_{avg}$ between emission source and each sampled location versus distance from plume core defined as maximum [CO] in each transect. Data are colored by estimated physical age.

1. South Sugarloaf Fire: vertical resolution of a wide plume

The South Sugarloaf Fire plume, sampled in northern Nevada near the Idaho border on 26 August, 2018, differed from the Taylor Creek plume in several ways. The fire was active over a larger area, leading to a plume approaching 100 km wide in some locations. Moreover, the South Sugarloaf plume remained in the boundary layer and formed a plume that was more than one km in height from roughly 3.6–4.6 km ASL, which made it possible to sample vertically-stacked crosswind transects to investigate vertical NEMR gradients (see Fig. S7). The maximum HONO mixing ratios were not as high as Taylor Creek, but were more

in line with other fires sampled during WE-CAN (Peng et al., 2020). Also, the HONO photolysis rates were generally slower, especially in the darker plume core, in part because this plume was sampled when clouds were present aloft. The clouds were not interacting with the smoke but led to slower photolysis rates within and around the plume. While the Taylor Creek plume was sampled only during midafternoon, the South Sugarloaf fire was sampled from midday through nearly sunset (14:00-20:00 LT) due to the closer proximity to the aircraft base of operations. This more extended sampling allowed an investigation of how vertical and horizontal crosswind gradients evolved as day transitioned to night.

Dilution-corrected gradients were observed between the cores and edges of vertically stacked crosswind transects in the South Sugarloaf fire, four of which are shown in Fig. 3. These transects were sampled during midday (1440-1540 LT) at an estimated physical age of 76 min. Compounds such as $C_6H_6O_1$, $C_6H_6O_2$, and HONO were depleted on the edges of each transect, while O_3 and $C_3H_4O_3$ were enhanced. Gradients can be observed by plotting NEMRs as a function of excess CO, where the densest part of the plume has the highest excess CO. An example is shown in Fig. S8 for a fresh transect. Vertically stacked measurements of HCN, CO, and calculated $[OH]_{avg}$ are shown in Fig. S9 for comparison. $[OH]_{avg}$ is again calculated from $C_6H_6O_2$ and CO, shown for comparison with Fig. 2 though it may be less reliable due to a larger possible influence from non-OH oxidation chemistry in the darker plume conditions.

NEMR gradients in the vertical are observed as well. HONO was most depleted in the top transect and along the edges, owing to the higher j_{HONO} values in those locations. The highest HONO mixing ratios were found not in the lowest altitude transect as j_{HONO} might suggest, but in the upper middle transect where both j_{HONO} was low and [CO] was high. Either the smoke in the lowest crosswind transects experienced higher j_{HONO} values along their trajectory between emission and being sampled, or the HONO emission factor was higher for smoke that rose to a higher altitude, consistent with more intense combustion conditions being a source of HONO (Peng et al., 2020). While the narrow Taylor Creek plume might reasonably be assumed to have a single emission factor for each compound, the much broader South Sugarloaf Fire likely resulted from a more diverse mix of emission processes that may not have been well-mixed during transport. Some variation in dilution corrected HCN was observed, though generally it remained constant across each transect (Fig. S9). Reactive organic compounds such as $C_6H_6O_1$ and $C_6H_6O_2$ followed the trend of HONO of being most concentrated in the core of the plume with highest [CO]. These compounds were depleted above, below, and to the sides of that core, while O_3 was enhanced in those same locations relative to the core. $C_3H_4O_3$ was enhanced more towards the lower altitudes and on the edges.

Several other vertically stacked transects of the South Sugarloaf fire plume were conducted at various physical ages and times of day, which further illustrate the variety of possible gradients. These examples, discussed in Sect. S4, include two sets of transects sampled at the same estimated physical age of 47 min. One

set was sampled during midday and captured strong vertical gradients in the top-most part of the plume (Fig. S10), while the other set was sampled near sunset and showed conditions with O_3 depletion and the lack of any gradients due to slow HONO photolysis (Fig. S11). These examples highlight the need to consider the time of day when wildfire emissions occur.

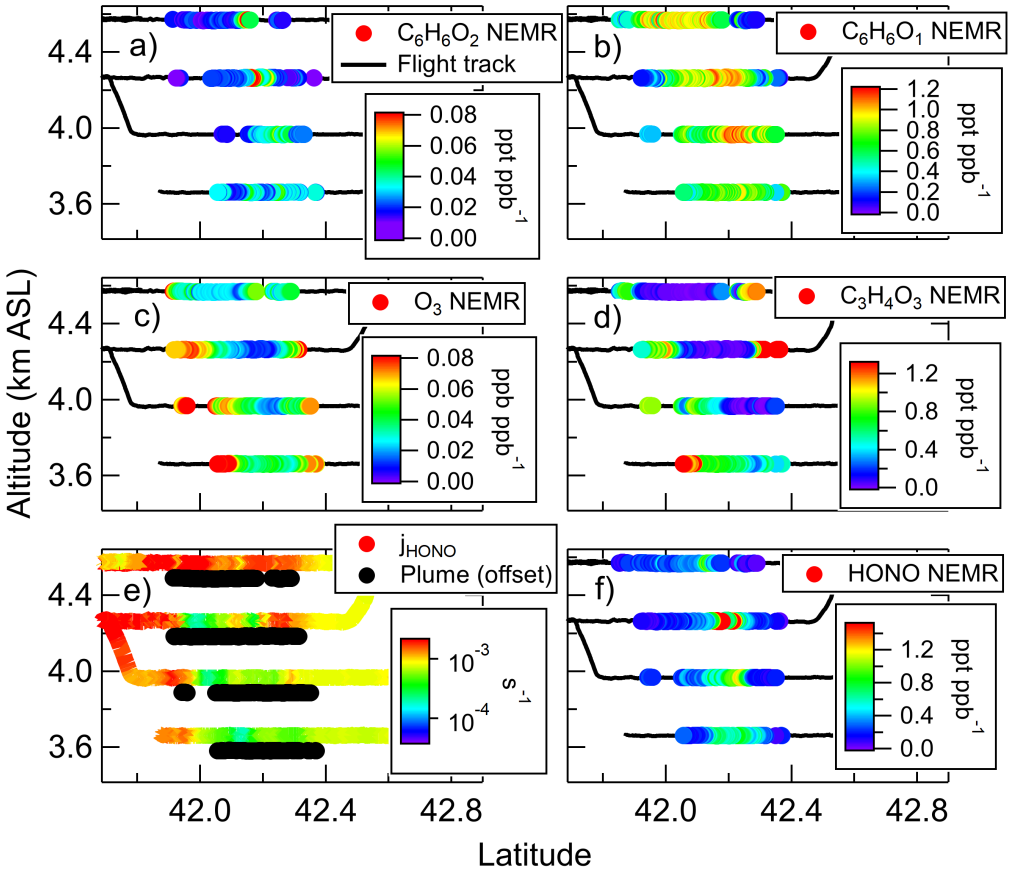

Figure 3. Measurements in four vertically stacked transects of the South Sugarloaf fire, sampled at an average est. physical age of 76 min from 1450-1550 LT. Gradients are observed in both horizontal and vertical directions. The plume center is defined by enhanced a) $C_6H_6O_2$, b) $C_6H_6O_1$, and f) HONO. c) O_3 and d) $C_3H_4O_3$ are enhanced on the edges, top, and bottom of the plume. Measured e) j_{HONO} is shown along the entire flight track, with the plume location

indicated with offset black dots for comparison.

1. Gradient strength depends on time of day at emission and sampling

The case studies above illustrate how observed NEMR gradients are dependent on the specific photochemical conditions experienced within each plume. To investigate the representativeness of those examples, we performed an analysis of gradients observed in all crosswind transects in coherent plumes (at least three physical ages sampled) sampled during the WE-CAN field campaign with estimated physical ages up to six hours. The gradient magnitude was defined as the difference between the NEMR of the plume core (defined as where [CO] was above the 90^{th} percentile in each crosswind transect) versus the transect average NEMR. Since the above examples suggested that gradients are more tied to the extent of chemical aging rather than physical age, this analysis used the ratio of estimated physical age to the lifetime of HONO against photolysis in the plume core ($_{\mathrm{HONO,core}}$), calculated as the inverse of the measured $j_{\mathrm{HONO,core}}$ in each transect. Values less than one indicate chemically fresh plumes where HONO largely has not yet been photolyzed, while larger values indicate more chemically aged plumes. This calculation does not take into account the history of $j_{\mathrm{HONO,core}}$ between emission and measurement (generally increasing with dilution while decreasing as the sun sets), but still provides a reasonable estimate of relative chemical age for these plumes in the first several hours after emission.

In Fig. 4, we show the gradient magnitude as a function of this chemical age metric for several compounds, with data also colored by the solar zenith angle (SZA) at the time of emission. Broadly, fast reacting compounds like $C_6H_6O_2$, HONO, and $C_7H_8O_2$ (Fig. S12) showed positive gradients (depleted on edges versus core) in chemically fresh plumes and near zero gradients in aged plumes where the compounds were depleted throughout the plumes. Oxidation products like O_3 and $C_3H_4O_3$ tended to have negative gradients (enhanced on edges versus core). Compounds that were reactive but not enough to be fully depleted in the first six hours of physical aging, like $C_6H_6O_1$, showed positive gradients across the range of chemical ages, while compounds that were unreactive on these time scales like HCN showed no gradients (as expected; Fig. S12).

Focusing on the chemically fresh plumes where the estimated physical age was less than $_{\mathrm{HONO,core}}$, the gradient strengths depended on SZA at emission. The plumes emitted closest to midday with the lowest SZA showed the strongest gradients, positive for reactive compounds and negative for oxidation products. When plumes were emitted late in the day at higher SZA, little to no gradients were observed for all compound types.

Trends are also observed when comparing gradient magnitudes to absolute NEMR magnitudes, as shown in Fig. S13 as a function of physical age. For the fastest reacting compounds with photolysis or reaction lifetimes on the order of 30 min or less (e.g., $C_6H_6O_2$, HONO, and $C_7H_8O_2$), the core NEMR was up to 50% higher than the transect average NEMR in the chemically freshest transects. The core NEMR values in the chemically freshest plumes will most

closely represent the true ER values. For compounds that react or form on the time scale of one to several hours (e.g., $C_6H_6O_1$, $C_3H_4O_3$, O_3, etc.), the core NEMR was typically up to 20% higher than the transect average and the gradients lasted out to longer physical ages.

We expect there are other fast reacting or fast forming compounds that are not measureable in this campaign because, e.g., the I^- CIMS cannot separate isomers with different gradients, or an oxidation product is formed that rapidly partitions to the unspeciated particle phase.

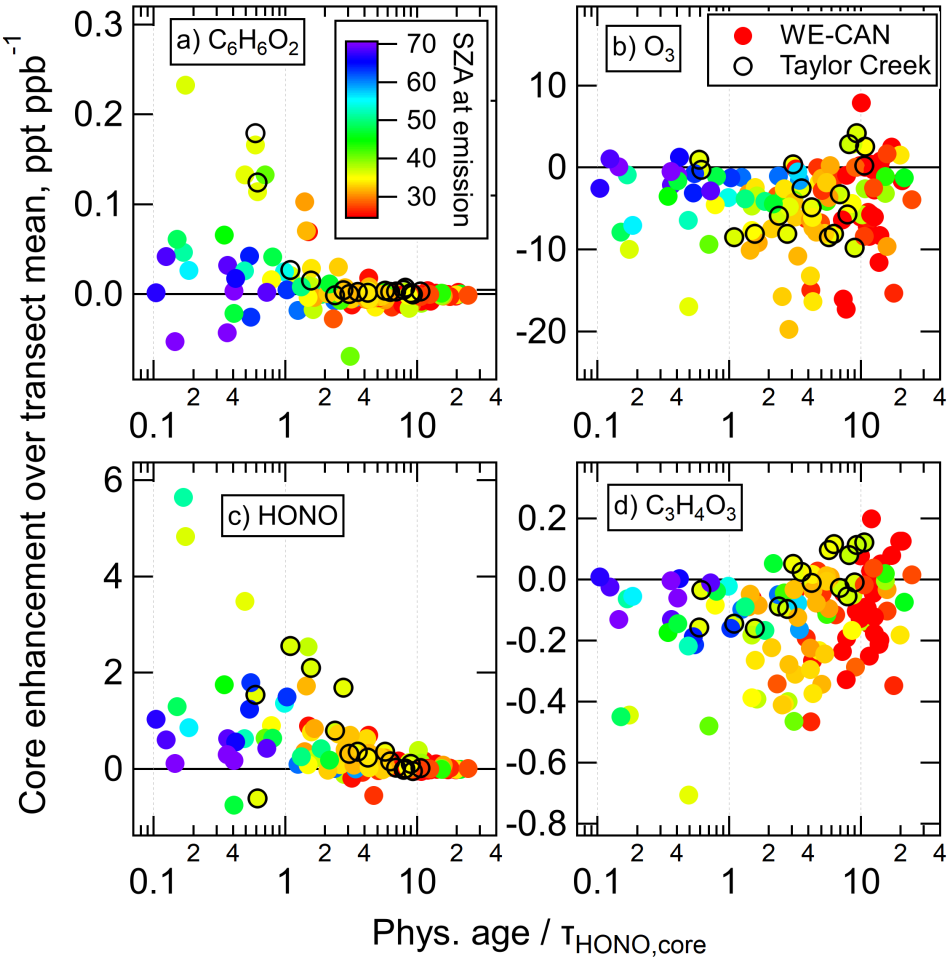

Figure 4. Enhancements of NEMRs in plume cores (average where [CO] > 90th

percentile) relative to transect mean NEMRs for all WE-CAN transects, for a) $C_6H_6O_2$, b) O_3, c) HONO, and d) $C_3H_4O_3$. The Taylor Creek plume transects are highlighted.

1. Conclusions

By sampling crosswind transects of wildfire plumes at different physical ages and altitudes with high spatial resolution, spatial variations in plume oxidation chemistry were observed during the WE-CAN aircraft campaign. NEMR gradients were strongest for the most reactive compounds such as HONO and $C_6H_6O_2$ in the chemically freshest plume transects during midday. In the South Sugarloaf fire, vertical gradients were also observed around the plume core. Gradients appeared to be driven by variations in j_{HONO} on diffuse plume edges or tops versus concentrated plume cores during midday plumes. During late evening plumes (and likely nighttime plumes) when the photolysis lifetime of HONO became long even on plume edges, gradients were no longer observed as the OH oxidation chemistry slowed down. This suggests that the fate of wildfire emissions may be dramatically different depending on the time of day at emission.

These measurements indicate that averaging entire transects into single NEMR values may lead to up to 50% underestimated ERs for the most reactive compounds (smaller amounts for less reactive compounds), and overestimated ERs for oxidation products in fresh wildfire plumes. Using screening methods such as using the top percentile of data may be more accurate for some applications, but should be combined with other information about the chemical age of the smoke. Plume gradients should also be considered when comparing *in situ* measurements with 0D plume models.

Acknowledgments and Data

B.B.P., Q.P., and J.A.T. were supported by the US National Science Foundation (NSF; AGS-1652688) and National Oceanic and Atmospheric Administration (NOAA; NA17OAR4310012). This research was supported by the U.S. NSF (AGS-1650786 and AGS-1650275). WE-CAN data (merge R4) is available at https://www-air.larc.nasa.gov/cgi-bin/ArcView/firexaq?MERGE=1. We thank everyone involved in planning and operations during WE-CAN. This material is based upon work supported by the National Center for Atmospheric Research, which is a major facility sponsored by the NSF under Cooperative Agreement No. 1852977. The data were collected using NSF's Lower Atmosphere Observing Facilities, which are managed and operated by NCAR's Earth Observing Laboratory. The operational and scientific support from NCAR's Earth Observing Laboratory and Research Aircraft Facility is gratefully acknowledged.

References

Abatzoglou, J. T., & Williams, A. P. (2016). Impact of anthropogenic climate change on wildfire across western US forests. *Proceedings of the National Academy of Sciences*, *113*(42), 11770–11775. https://doi.org/10.1073/pnas.1607171113Akagi,

S. K., Craven, J. S., Taylor, J. W., McMeeking, G. R., Yokelson, R. J., Burling, I. R., et al. (2012). Evolution of trace gases and particles emitted by a chaparral fire in California. *Atmospheric Chemistry and Physics*, *12*(3), 1397–1421. https://doi.org/10.5194/acp-12-1397-2012Andreae, M. O. (2019). Emission of trace gases and aerosols from biomass burning – an updated assessment. *Atmospheric Chemistry and Physics*, *19*(13), 8523–8546. https://doi.org/10.5194/acp-19-8523-2019Atkinson, R., & Arey, J. (2003). Atmospheric Degradation of Volatile Organic Compounds. *Chemical Reviews*, *103*(12), 4605–4638. https://doi.org/10.1021/cr0206420Atkinson, R., Baulch, D. L., Cox, R. A., Hampson, R. F., Kerr (Chairman), J. A., & Troe, J. (1989). Evaluated Kinetic and Photochemical Data for Atmospheric Chemistry: Supplement III. IUPAC Subcommittee on Gas Kinetic Data Evaluation for Atmospheric Chemistry. *Journal of Physical and Chemical Reference Data*, *18*(2), 881–1097. https://doi.org/10.1063/1.555832Balch, J. K., Bradley, B. A., Abatzoglou, J. T., Nagy, R. C., Fusco, E. J., & Mahood, A. L. (2017). Human-started wildfires expand the fire niche across the United States. *Proceedings of the National Academy of Sciences of the United States of America*, 201617394. https://doi.org/10.1073/pnas.1617394114Burkholder, J. B., Sander, S. P., Abbatt, J., Barker, J. R., Cappa, C., Crounse, J. D., et al. (2019). *Chemical Kinetics and Photochemical Data for Use in Atmospheric Studies: Evaluation No. 19. JPL Publication 19-5*. Pasadena, CA, USA. Retrieved from http://jpldataeval.jpl.nasa.gov/Coggon, M. M., Lim, C. Y., Koss, A. R., Sekimoto, K., Yuan, B., Gilman, J. B., et al. (2019). OH chemistry of non-methane organic gases (NMOGs) emitted from laboratory and ambient biomass burning smoke: evaluating the influence of furans and oxygenated aromatics on ozone and secondary NMOG formation. *Atmospheric Chemistry and Physics*, *19*(23), 14875–14899. https://doi.org/10.5194/acp-19-14875-2019Decker, Z. C. J., Zarzana, K. J., Coggon, M., Min, K.-E., Pollack, I., Ryerson, T. B., et al. (2019). Nighttime Chemical Transformation in Biomass Burning Plumes: A Box Model Analysis Initialized with Aircraft Observations. *Environmental Science & Technology*, *53*(5), 2529–2538. https://doi.org/10.1021/acs.est.8b05359Dennison, P. E., Brewer, S. C., Arnold, J. D., & Moritz, M. A. (2014). Large wildfire trends in the western United States, 1984-2011. *Geophysical Research Letters*, *41*(8), 2928–2933. https://doi.org/10.1002/2014GL059576Garofalo, L. A., Pothier, M. A., Levin, E. J. T., Campos, T., Kreidenweis, S. M., & Farmer, D. K. (2019). Emission and Evolution of Submicron Organic Aerosol in Smoke from Wildfires in the Western United States. *ACS Earth and Space Chemistry*, *3*(7), 1237–1247. research-article. https://doi.org/10.1021/acsearthspacechem.9b00125de Gouw, J. A., Middlebrook, A. M., Warneke, C., Goldan, P. D., Kuster, W. C., Roberts, J. M., et al. (2005). Budget of organic carbon in a polluted atmosphere: Results from the New England Air Quality Study in 2002. *Journal of Geophysical Research*, *110*(D16), D16305. https://doi.org/10.1029/2004JD005623Higuera, P. E., & Abatzoglou, J. T. (2021). Record-setting climate enabled the extraordinary 2020 fire season in the western United States. *Global Change Biology*, *27*(1), 1–2. https://doi.org/10.1111/gcb.15388Higuera, P. E., Shuman, B. N., &

Wolf, K. D. (2021). Rocky Mountain subalpine forests now burning more than any time in recent millennia. *Proceedings of the National Academy of Sciences*, *118*(25), e2103135118. https://doi.org/10.1073/pnas.2103135118Hodshire, A. L., Ramnarine, E., Akherati, A., Alvarado, M. L., Farmer, D. K., Jathar, S. H., et al. (2021). Dilution impacts on smoke aging: evidence in Biomass Burning Observation Project (BBOP) data. *Atmospheric Chemistry and Physics*, *21*(9), 6839–6855. https://doi.org/10.5194/acp-21-6839-2021Jenkin, M. E., Young, J. C., & Rickard, A. R. (2015). The MCM v3.3.1 degradation scheme for isoprene. *Atmospheric Chemistry and Physics*, *15*(20), 11433–11459. https://doi.org/10.5194/acp-15-11433-2015Joo, T., Rivera-Rios, J. C., Takeuchi, M., Alvarado, M. J., & Ng, N. L. (2019). Secondary Organic Aerosol Formation from Reaction of 3-Methylfuran with Nitrate Radicals. *ACS Earth and Space Chemistry*, *3*(6), 922–934. https://doi.org/10.1021/acsearthspacechem.9b00068Juncosa Calahorrano, J. F., Lindaas, J., O'Dell, K., Palm, B. B., Peng, Q., Flocke, F., et al. (2021). Daytime Oxidized Reactive Nitrogen Partitioning in Western U.S. Wildfire Smoke Plumes. *Journal of Geophysical Research: Atmospheres*, *126*(4). https://doi.org/10.1029/2020JD033484Lebegue, B., Schmidt, M., Ramonet, M., Wastine, B., Yver Kwok, C., Laurent, O., et al. (2016). Comparison of nitrous oxide (N_2O) analyzers for high-precision measurements of atmospheric mole fractions. *Atmospheric Measurement Techniques*, *9*(3), 1221–1238. https://doi.org/10.5194/amt-9-1221-2016Liu, X., Huey, L. G., Yokelson, R. J., Selimovic, V., Simpson, I. J., Müller, M., et al. (2017). Airborne measurements of western U.S. wildfire emissions: Comparison with prescribed burning and air quality implications. *Journal of Geophysical Research: Atmospheres*, *122*(11), 6108–6129. https://doi.org/10.1002/2016JD026315McClure, C. D., & Jaffe, D. A. (2018). US particulate matter air quality improves except in wildfire-prone areas. *Proceedings of the National Academy of Sciences*, *115*(31), 7901–7906. https://doi.org/10.1073/pnas.1804353115O'Dell, K., Ford, B., Fischer, E. V., & Pierce, J. R. (2019). Contribution of Wildland-Fire Smoke to US PM 2.5 and Its Influence on Recent Trends. *Environmental Science & Technology*, *53*(4), 1797–1804. https://doi.org/10.1021/acs.est.8b05430Olariu, R. I., Barnes, I., Becker, K. H., & Klotz, B. (2000). Rate coefficients for the gas-phase reaction of OH radicals with selected dihydroxybenzenes and benzoquinones. *International Journal of Chemical Kinetics*, *32*(11), 696–702. https://doi.org/10.1002/1097-4601(2000)32:11<696::AID-KIN5>3.0.CO;2-NOlariu, R. I., Bejan, I., Barnes, I., Klotz, B., Becker, K. H., & Wirtz, K. (2004). Rate coefficients for the gas-phase reaction of NO_3 radicals with selected dihydroxybenzenes. *International Journal of Chemical Kinetics*, *36*(11), 577–583. https://doi.org/10.1002/kin.20029Palm, B. B., Liu, X., Jimenez, J. L., & Thornton, J. A. (2019). Performance of a new coaxial ion–molecule reaction region for low-pressure chemical ionization mass spectrometry with reduced instrument wall interactions. *Atmospheric Measurement Techniques*, *12*(11), 5829–5844. https://doi.org/10.5194/amt-12-5829-2019Palm, B. B., Peng, Q., Fredrickson, C. D., Lee, B. H., Garofalo, L. A., Pothier, M. A., et al. (2020). Quantification of organic aerosol and brown carbon evolution

in fresh wildfire plumes. *Proceedings of the National Academy of Sciences*, *117*(47), 29469–29477. https://doi.org/10.1073/pnas.2012218117Peng, Q., Palm, B. B., Melander, K. E., Lee, B. H., Hall, S. R., Ullmann, K., et al. (2020). HONO Emissions from Western U.S. Wildfires Provide Dominant Radical Source in Fresh Wildfire Smoke. *Environmental Science & Technology*, *54*(10), 5954–5963. https://doi.org/10.1021/acs.est.0c00126Permar, W., Wang, Q., Selimovic, V., Wielgasz, C., Yokelson, R. J., Hornbrook, R. S., et al. (2021). Emissions of Trace Organic Gases From Western U.S. Wildfires Based on WE-CAN Aircraft Measurements. *Journal of Geophysical Research: Atmospheres*, *126*(11). https://doi.org/10.1029/2020JD033838Radeloff, V. C., Helmers, D. P., Kramer, H. A., Mockrin, M. H., Alexandre, P. M., Bar-Massada, A., et al. (2018). Rapid growth of the US wildland-urban interface raises wildfire risk. *Proceedings of the National Academy of Sciences*, *115*(13), 3314–3319. https://doi.org/10.1073/pnas.1718850115Roberts, J. M., Fehsenfeld, F. C., Liu, S. C., Bollinger, M. J., Hahn, C., Albritton, D. L., & Sievers, R. E. (1984). Measurements of aromatic hydrocarbon ratios and NOx concentrations in the rural troposphere: Observation of air mass photochemical aging and NOx removal. *Atmospheric Environment (1967)*, *18*(11), 2421–2432. https://doi.org/10.1016/0004-6981(84)90012-XShetter, R. E., & Müller, M. (1999). Photolysis frequency measurements using actinic flux spectroradiometry during the PEM-Tropics mission: Instrumentation description and some results. *Journal of Geophysical Research: Atmospheres*, *104*(D5), 5647–5661. https://doi.org/10.1029/98JD01381van der Werf, G. R., Randerson, J. T., Giglio, L., van Leeuwen, T. T., Chen, Y., Rogers, B. M., et al. (2017). Global fire emissions estimates during 1997–2016. *Earth System Science Data*, *9*(2), 697–720. https://doi.org/10.5194/essd-9-697-2017Westerling, A. L. (2016). Increasing western US forest wildfire activity: sensitivity to changes in the timing of spring. *Philosophical Transactions of the Royal Society B: Biological Sciences*, *371*(1696), 20150178. https://doi.org/10.1098/rstb.2015.0178Wiedinmyer, C., Akagi, S. K., Yokelson, R. J., Emmons, L. K., Al-Saadi, J. A., Orlando, J. J., & Soja, A. J. (2011). The Fire INventory from NCAR (FINN): a high resolution global model to estimate the emissions from open burning. *Geoscientific Model Development*, *4*(3), 625–641. https://doi.org/10.5194/gmd-4-625-2011Wolfe, G. M., Marvin, M. R., Roberts, S. J., Travis, K. R., & Liao, J. (2016). The Framework for 0-D Atmospheric Modeling (F0AM) v3.1. *Geoscientific Model Development*, *9*(9), 3309–3319. https://doi.org/10.5194/gmd-9-3309-2016Yokelson, R. J., Goode, J. G., Ward, D. E., Susott, R. A., Babbitt, R. E., Wade, D. D., et al. (1999). Emissions of formaldehyde, acetic acid, methanol, and other trace gases from biomass fires in North Carolina measured by airborne Fourier transform infrared spectroscopy. *Journal of Geophysical Research*, *104*(D23), 30109. https://doi.org/10.1029/1999JD900817Yokelson, R. J., Crounse, J. D., DeCarlo, P. F., Karl, T., Urbanski, S., Atlas, E., et al. (2009). Emissions from biomass burning in the Yucatan. *Atmospheric Chemistry and Physics*, *9*(15), 5785–5812.

Geophysical Research Letters

Supporting Information for

Spatially resolved photochemistry impacts emissions estimates in fresh wildfire plumes

Brett B. Palm[1,*,#], Qiaoyun Peng[1], Samuel R. Hall[2], Kirk Ullmann[2], Teresa L. Campos[2], Andrew Weinheimer[2], Deedee Montzka[2], Geoffrey Tyndall[2], Wade Permar[3], Lu Hu[3], Frank Flocke[2], Emily V. Fischer[4], Joel A. Thornton[1]

[1]Department of Atmospheric Sciences, University of Washington, Seattle, WA, USA 98195

[2]Atmospheric Chemistry Observations and Modeling Laboratory, National Center for Atmospheric Research, Boulder, CO, USA 80301

[3]Department of Chemistry and Biochemistry, University of Montana, Missoula, MT, USA 59812

[4]Department of Atmospheric Science, Colorado State University, Fort Collins, CO, USA 80523

[@]Now at: Atmospheric Chemistry Observations and Modeling Laboratory, National Center for Atmospheric Research, Boulder, CO, USA 80301

[#]Corresponding author: Brett B. Palm (bbpalm@ucar.edu)

Contents of this file

S1 Instrument and measurement details

The I^- CIMS measured a variety of organic and inorganic compounds, including HONO, HCN, several likely phenolic compounds, and a suite of other oxidized organic compounds. Ambient air was sampled at 20 lpm through a ¾" OD, ~50 cm long PTFE Teflon tube into the cabin. Air was then subsampled at 2 slpm into the CIMS through a custom inlet (Palm et al., 2019). Data was collected at 2 Hz and averaged to 1 Hz for use. The calibration factors used for each compound are described in Palm et al. (2020). $C_3H_4O_3$ was not calibrated due to a lack of knowledge of the sampled isomer composition, so mixing ratios were calculated using a typical calibration value of 5 counts per second per million reagent ions per pptv. $C_6H_6O_2$ was screened to remove measurement "tails" that result from that compound interacting with inlet surfaces (see Palm et al., 2019), by removing any $C_6H_6O_2$ data where $C_6H_6O_1$ (a compound with minimal inlet surface interactions) had decayed to below 20% of its peak in each transect. The other I^- CIMS compounds used here are more volatile and thus did not have such inlet artifacts.

CO was sampled using a commercial Mini-QCL tunable diode laser infrared absorption spectrometer (Lebegue et al., 2016). To optimize measurement accuracy, the spectrometer optical bench was continuously purged with synthetic zero grade air from which CO had been scrubbed to contain less than 1 ppbv. N_2O was also measured by the Mini-QCL, and was quantified in the purge gas at typically less than 0.3 ppbv. The N_2O purge gas concentration was included in spectral fit calculations to better reproduce the spectral background. The CO measurement had a precision of 0.1 ppbv with a 2 s temporal resolution and an accuracy of +/- 0.6 ppbv. The photolysis rate of HONO (j_{HONO}) was calculated from actinic flux measurements taken by the HIAPER Atmospheric Radiation Package (HARP; Shetter & Müller, 1999). Ozone (O_3) was measured by a chemiluminescense instrument at 1 Hz, with an accuracy of 5%. A proton transfer reaction time-of-flight mass spectrometer (PTR-ToF-MS) was used to measure a suite of volatile organic compounds (VOCs), including C_6H_6 and C_7H_8 used here (Permar et al., 2021). The data from various instruments were aligned in time by maximizing correlations of non-reactive compounds in the plumes.

The physical age of each transect was estimated by dividing the average distance from each transect to the fire source location by the average wind speed measured in the plume. The solar zenith angle (SZA) at time of emission (sampled time minus physical age) was calculated for each sampled latitude and longitude using the NOAA Solar Calculator, based on equations from *Astronomical Algorithms*, by Jean Meeus.

NEMRs were calculated as background-subtracted ratios of various compounds to CO. The background values were determined by averaging out-of-plume measurements from before and/or after each transect (typically 15 s on each side) to get a single background value per transect for each compound. Some transects did not fully exit the plume, so their background values were determined using data from only one side of the transect. Such transects were identified by comparing with the backgrounds determined in nearby transects and looking for outliers. While the South Sugarloaf fire was confined to (and diluted with) the boundary layer, the airplane occasionally transitioned into free tropospheric air while sampling the background before or after some transects sampled at the very top of the plume. Free tropospheric air was

identified by, e.g., low mixing ratios of water vapor, formic acid, and a variety of other compounds. This air was not representative of the air with which the plume was diluting, so such measurements were not included as background values. The Taylor Creek Fire plume, on the other hand, was injected into (and predominantly diluted with) the free troposphere, so background values were selected from free tropospheric air before and after each transect.

S2 Methodology for estimating $[OH]_{avg}$ in the Taylor Creek Fire plume

In non-diluting systems, e.g., batch chamber experiments of photochemical aging, OH concentrations can be derived by measuring the decay of a single compound and applying reaction kinetics. In diluting systems, e.g., urban downwind or wildfire plumes, the photochemical aging can be spatially inhomogeneous and difficult to estimate because of dilution and variations in parameters such as actinic flux. Previous studies of urban plumes have estimated photochemical age at various locations downwind by analyzing the change in the ratio of two compounds with a known emission ratio (de Gouw et al., 2005; Roberts et al., 1984). Dilution acts equally on the concentration of both compounds, so a change in the ratio indicates oxidation chemistry (or other formation/loss processes) when the two compounds have different reactivities. For systems where physical age can be estimated (e.g., wildfire or other point sources), the photochemical age estimated from changing ratios can be converted to average oxidant concentrations.

Past studies of urban air have used various organic compounds but not CO (de Gouw et al., 2005; Roberts et al., 1984), because CO is emitted by many urban sources at different rates. For wildfires, CO emissions can be characterized directly with measurements for individual fires, so it can be used as one of the two compounds.

To estimate the fractional fate of $C_6H_6O_2$ to reaction with OH, NO_3, or O_3 in the Taylor Creek Fire plume, we used the Framework for 0-D Atmospheric Modeling (F0AM) box model with the Master Chemical Mechanism (MCM) v3.3.1 chemical mechanism (Jenkin et al., 2015; Wolfe et al., 2016). The MCM is a near-explicit chemical mechanism with detailed gas-phase chemical processes for a variety of compounds, including 142 primarily emitted non-methane VOCs and their oxidation products. Additional mechanisms were added, including the recent mechanism development from laboratory measurements for heterocyclic hydrocarbons (like furans) and phenolics, which are found to significantly contribute to secondary product formation in biomass burning plumes (Coggon et al., 2019; Decker et al., 2019; Joo et al., 2019).

In Fig. S3, we show the fractional loss of $C_6H_6O_2$ to each of the oxidants when initializing the model with mixing ratios measured in the core (95^{th} percentile [CO]) or the edges (30^{th} percentile [CO]) of the plume. We estimate that 28% of $C_6H_6O_2$ will react with NO_3 in the core, and 10% on the edges. O_3 accounts for a negligible several percent, with the remainder going to reaction with OH. When estimating the fractional fates across the entire plume for the purposes of estimating $[OH]_{avg}$ in Sect. 3.1.2, we assumed 75% of $C_6H_6O_2$ reacted with OH in the Taylor Creek plume. The uncertainties associated with this assumption are likely small relative to those in the sensitivity analysis of the initial $C_6H_6O_2$ to CO ratio in Sect S3. This analysis also suggests that reaction with OH, not with NO_3, was the cause of the measured

crosswind gradients, since NO_3 was found to account for less reaction on the edges versus the plume core.

S3 Sensitivity analysis

Since it was not possible to sample the exact emission ratios of highly reactive compounds such as $C_6H_6O_2$ in authentic wildfires from the aircraft platform, the initial ratio of $C_6H_6O_2$ to CO is a source of uncertainty. In Sect. 3.1.2, we used an initial ratio of 1. The evolution of this ratio with plume age is shown in Fig. S6b. In Fig. S5, we show the calculations of $[OH]_{avg}$ using initial ratios of 0.7 and 1.5 to show the sensitivity of this calculation to the initial ratio. The estimated $[OH]_{avg}$ in the freshest transects varies by up to approximately a factor of two, but the gradients are robust. The $[OH]_{avg}$ in aged transects is less sensitive to the initial ratio. We also investigated the use of different compound ratios, including $C_6H_6O_1$ to CO, $C_6H_6O_2$ to $C_6H_6O_1$, and C_7H_8 to C_6H_6 as shown in Fig. S6. None of the compounds except $C_6H_6O_2$ were expected to react appreciably with oxidants other than OH. The results were similar, with the exception that the fresh plume gradients were not as clear when $C_6H_6O_2$ is not one of the compounds used. The likely reason for this behavior is that $C_6H_6O_2$ is the only compound that reacts with OH fast enough to form measureable gradients on this time scale. After an estimated 22 min of physical age in the freshest transects, the fraction of $C_6H_6O_2$ remaining for $[OH]_{avg}$ values of 1.0×10^7 and 4×10^6 molecules cm^{-3} (plume edges versus core) is expected to be 30% and 62%, which is a measurable difference in the freshest crosswind transects. For $C_6H_6O_1$, we expect 73% and 88% remaining, which is similar to the expected measurement precision and other possible uncertainties (e.g., any variable emissions between core and edge). For C_7H_8, 94% and 97% are expected, which are indistinguishable in a single crosswind transect to within uncertainties, and C_6H_6 is even less reactive. Therefore, $C_6H_6O_2$ was the best available compound for calculating $[OH]_{avg}$ in the highly reactive and fresh Taylor Creek plume, and compounds such as C_7H_8 and C_6H_6 are not suitable for quantifying gradients on such short time scales.

S4 Additional vertically stacked transects in the South Sugarloaf fire

Several other vertically stacked transects of the South Sugarloaf fire plume were conducted in addition to those in Sect. 3.2. In Fig. S10, the upper two crosswind transects through the plume sampled at an age of 47 min from 1415-1445 LT clearly show steep vertical gradients in HONO, $C_6H_6O_2$, and O_3 at the top of the plume. The uppermost transect appears to have skimmed close to the top of the plume, where photolysis rates were much higher than the other transect ~350 m lower. In Fig. S11, a stack of transects at the same 47 min age but sampled as the sun was setting at 1850-1925 LT illustrates how the observed gradients were changing as day became night. The j_{HONO} values were low even outside of the plume, and the gradients in reactive compounds such as HONO and $C_6H_6O_2$ were much smaller, indicating OH production and associated chemistry were greatly slowed. In fact, O_3 was depleted in all locations inside the plume relative to background air in these evening transects, but especially in the denser portion of the plume at higher altitudes. Fig. S11 illustrates the behavior that is likely to be observed in wildfire plumes that are emitted at/after sunset. The differences in observed gradients highlights the need to understand the different chemical and physical evolution of daytime and nighttime plumes to model the downwind effects of emissions occurring throughout the day and night.

Figure S1. Images from the forward facing camera on the C-130 aircraft showing how the Taylor Creek Fire plume injected above the smoke-filled boundary layer into the free troposphere. The image on the left shows the plume shortly after injection, and the image on the right shows the evolution of the plume approximately 90 minutes later.

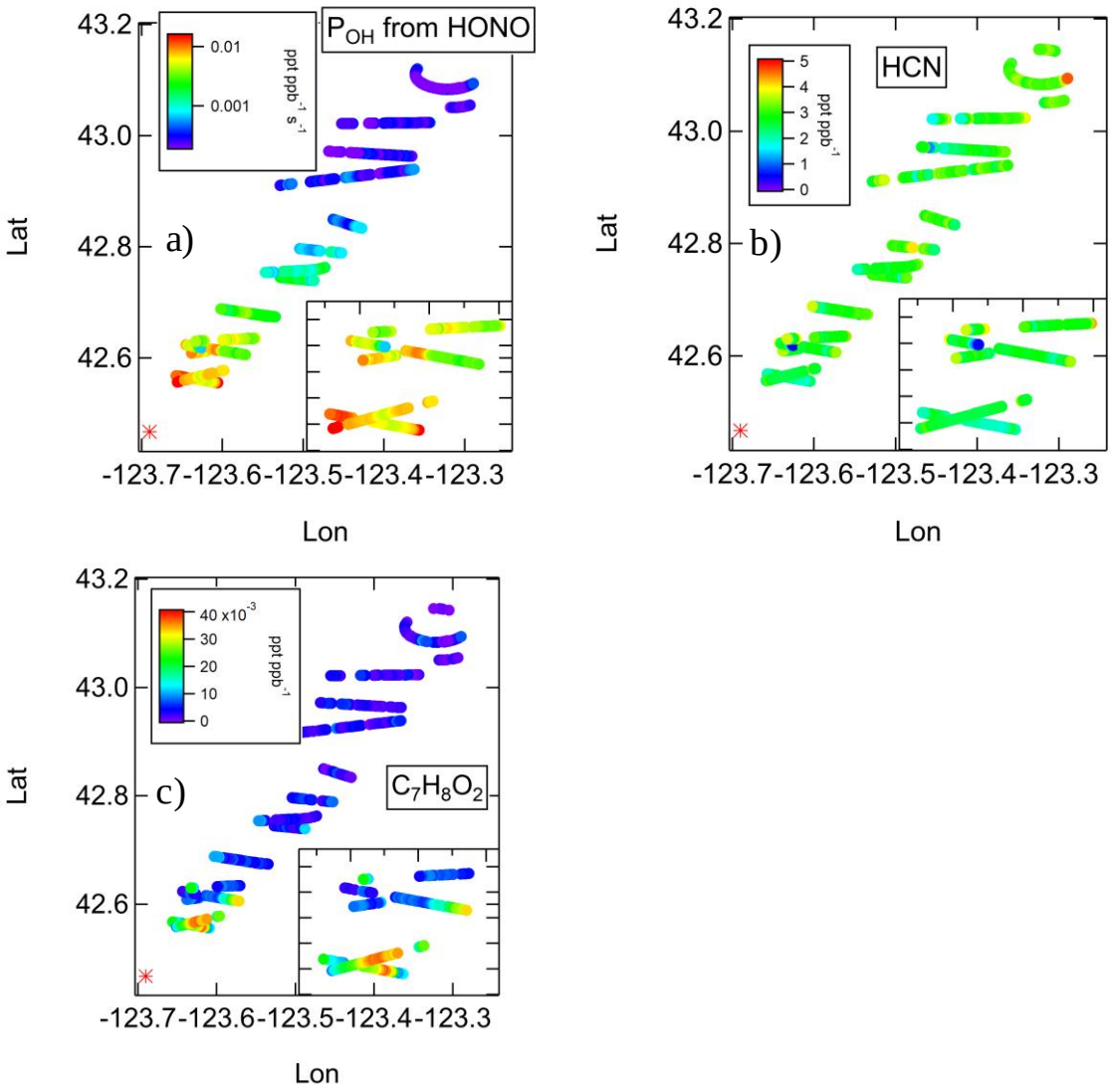

Figure S2. Plume transects in the Taylor Creek fire, showing spatial variations in a) the dilution-corrected production rate of OH from HONO photolysis, and the NEMRs of b) HCN and c) $C_7H_8O_2$. The insets show the first five transects in greater detail. Gradients were not observed for HCN, in contrast to the NEMRs of reactive compounds shown in Fig. 1.

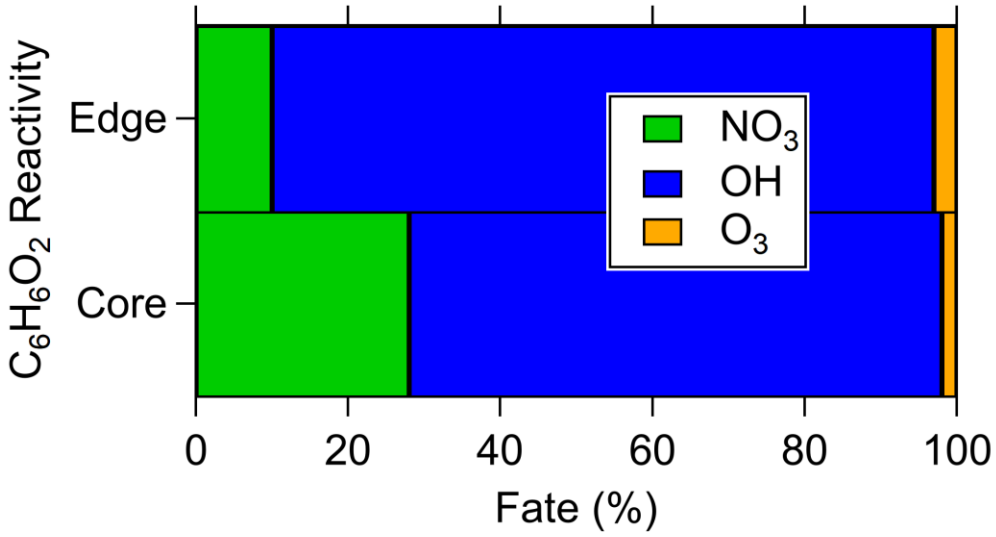

Figure S3. Percentage of reactivity of $C_6H_6O_2$ to oxidants in the Taylor Creek Fire plume. The reactivity was modeled using the F0AM box model when initializing the model with mixing ratios measured in the plume core (95th percentile [CO]) or on the plume edges (30th percentile values).

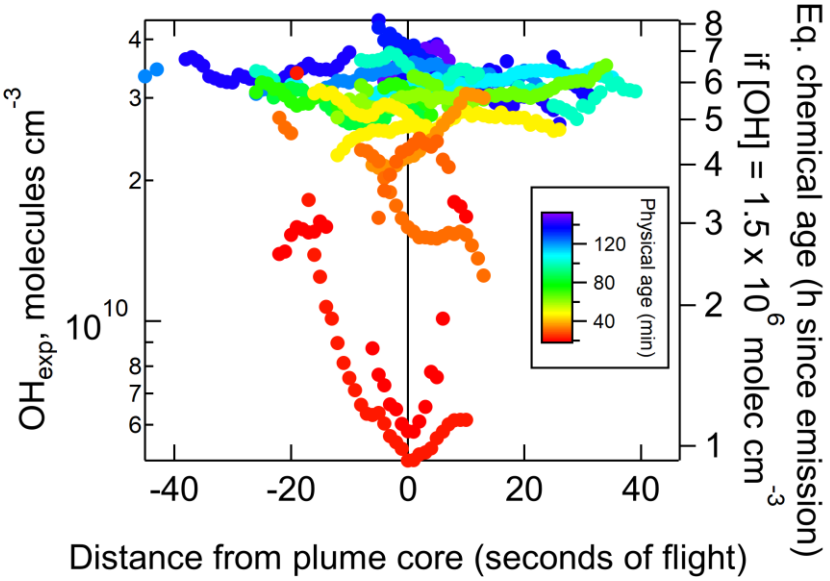

Figure S4. OH_{exp} at each sampled location in the Taylor Creek Fire plume, as a function of distance from the plume core. Data are colored by estimated physical age.

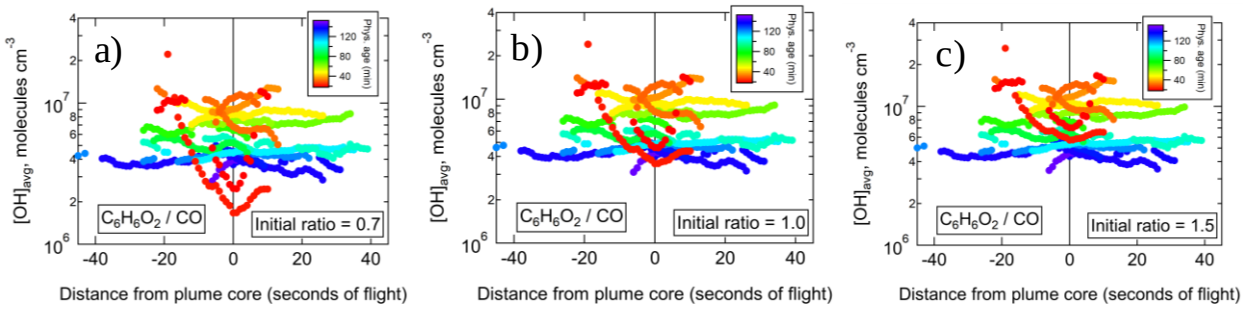

Figure S5. Calculations of $[OH]_{avg}$ in the Taylor Creek plume using initial $C_6H_6O_2$ to CO ratios of a) 0.7, b) 1, same as Fig. 2b, and c) 1.5. Data are colored by estimated physical age. This sensitivity analysis illustrates the absolute magnitude of $[OH]_{avg}$ varies by up to a factor of two over this range of initial ratios, but the existence of crosswind gradients and the evolution with plume age is robust.

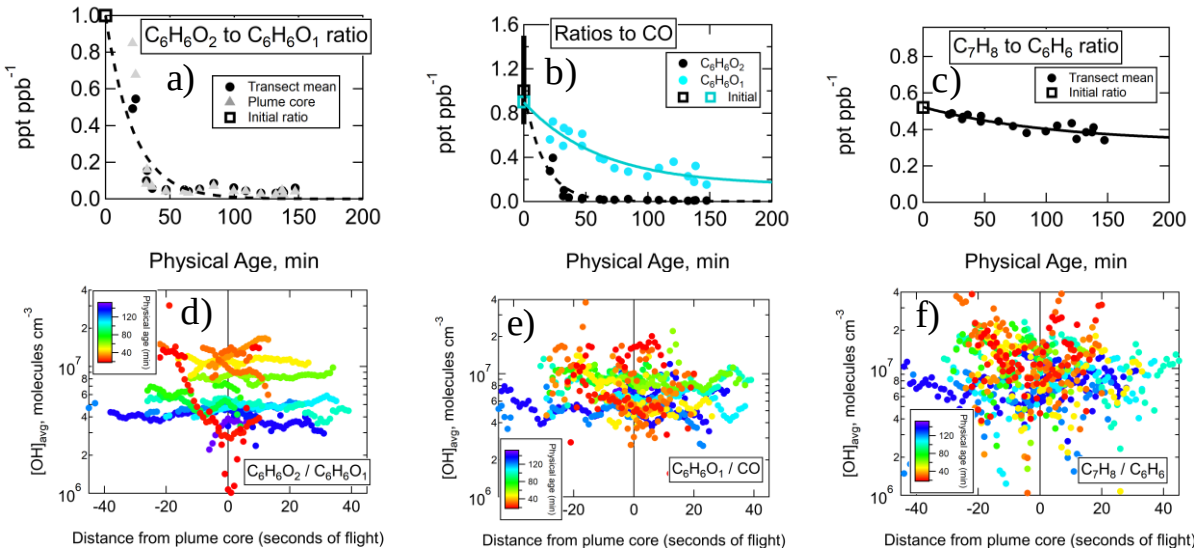

Figure S6. a, b, and c) The derivation of initial ratios, and d, e, and f) calculations of $[OH]_{avg}$ in the Taylor Creek plume using different compound ratios, for comparison to Fig. 2. See Sect. S3 for discussion.

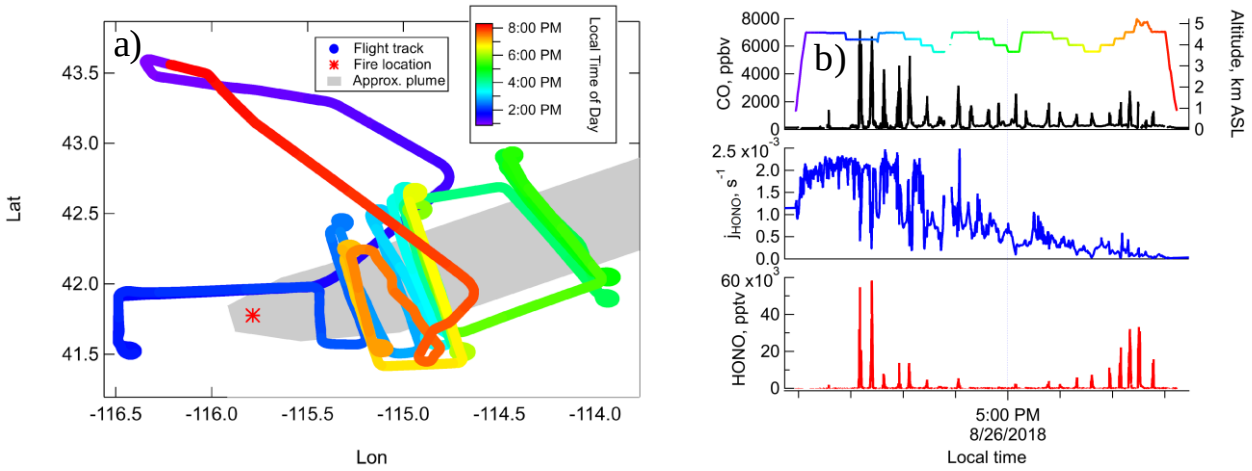

Figure S7. a) Flight track for the South Sugarloaf fire on Aug. 26, 2018, colored by local time of day and showing approximate fire and plume locations, and b) measurements of altitude, CO, j_{HONO}, and HONO, illustrating the changing photochemical conditions during the time of plume sampling. Altitude is also colored by local time of day.

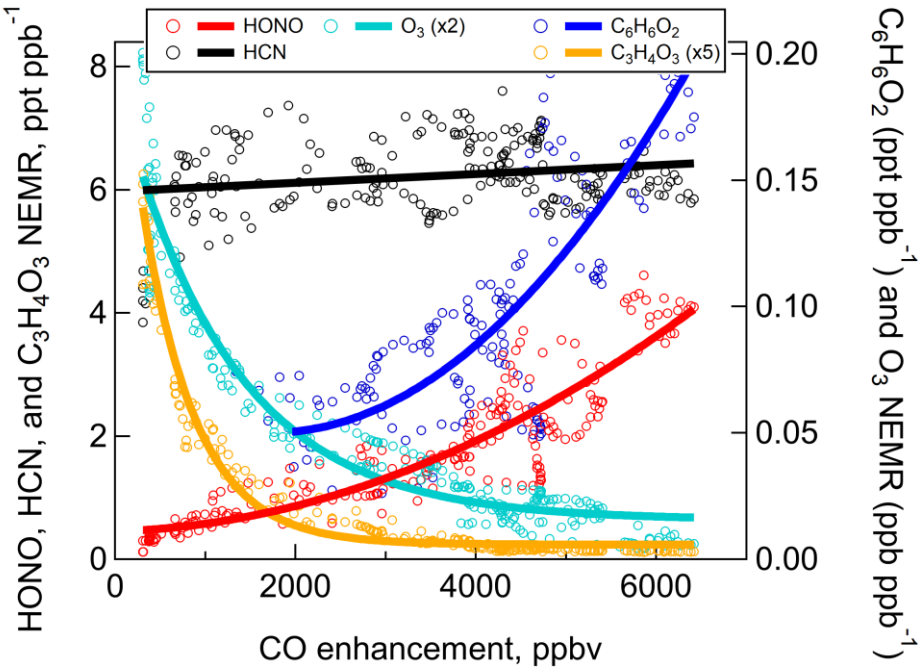

Figure S8. Gradients in several compounds as a function of CO enhancement above background in a crosswind transect of the South Sugarloaf fire plume. The highest CO enhancements are near the dark plume center, and CO enhancement decreases due to dilution on plume edges. This transect was sampled at an est. physical age of 44 min at 1420 LT. Reactive compounds such as HONO and $C_6H_6O_2$ are depleted on plume edges relative to center, due to faster photochemistry. Similarly, oxidation products such as O_3 and $C_3H_4O_3$ are enhanced on plume edges relative to center. Not all plume transects have the prototypical Gaussian shape, so plotting as a function of CO enhancement instead of distance from plume center (defined by highest CO) can be useful.

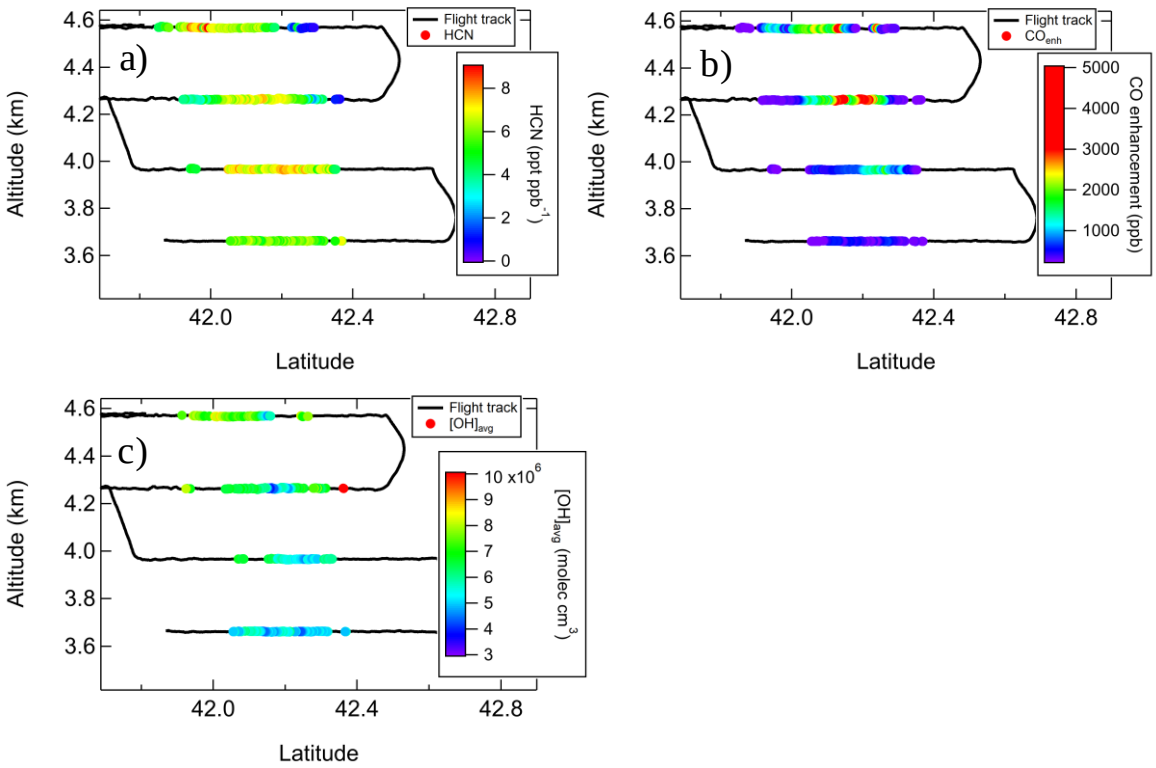

Figure S9. For comparison with Fig. 3, a) HCN, b) CO enhancement, and c) $[OH]_{avg}$ in four vertically stacked transects of the South Sugarloaf fire, sampled at an average est. physical age of 76 min from 1450-1550 LT. Relatively nonreactive compounds such as HCN remain roughly constant throughout each transect.

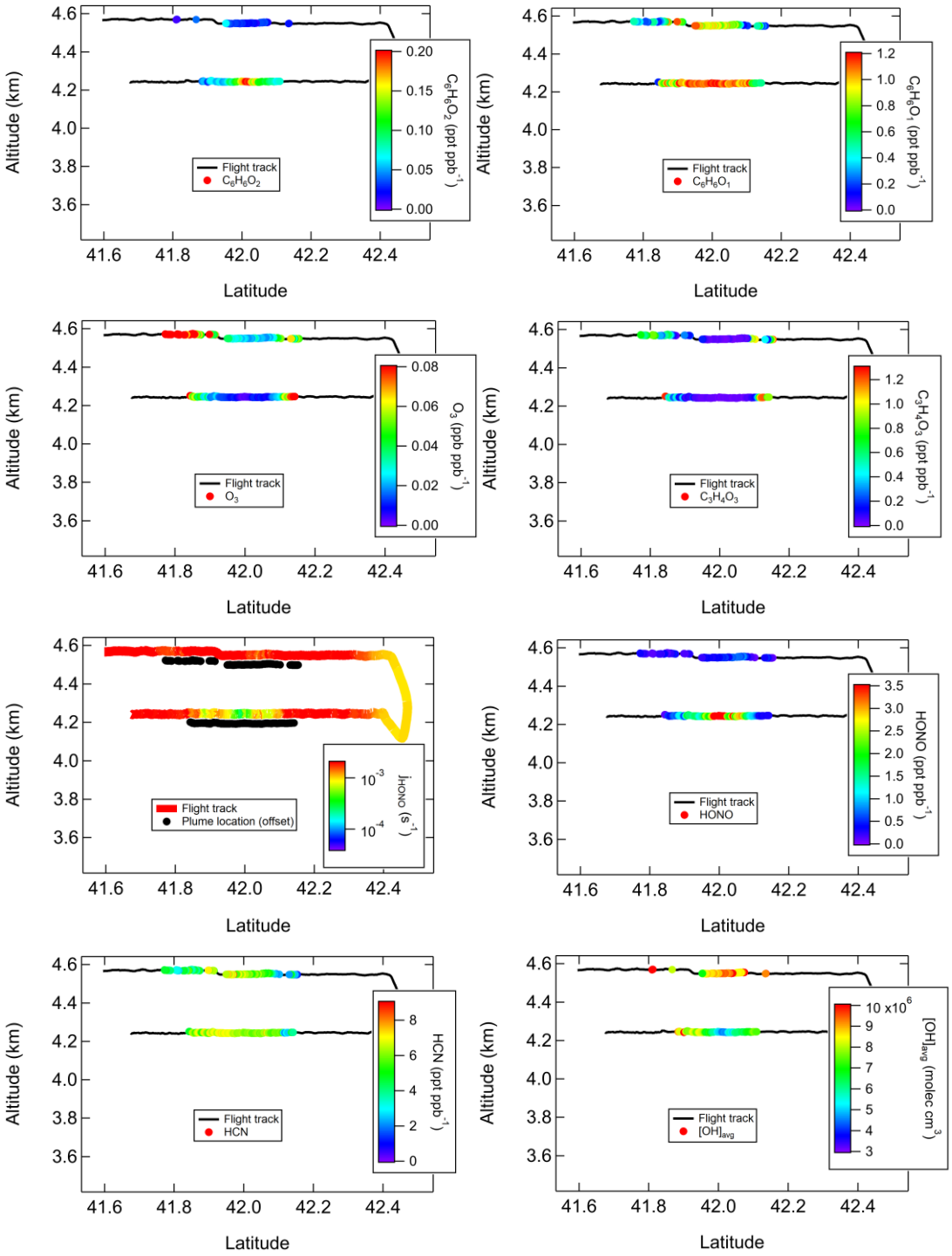

Figure S10. Various measurements in two vertically stacked transects in the South Sugarloaf fire sampled at an average physical age of 47 min, sampled from 1415-1445 LT. The upper transect had higher photolysis rates, leading to faster O_3 formation with more depleted HONO and $C_6H_6O_2$. This figure can be compared with Fig. S11, which shows a similar estimated physical age but sampled late in the day with different chemical conditions leading to weaker gradients.

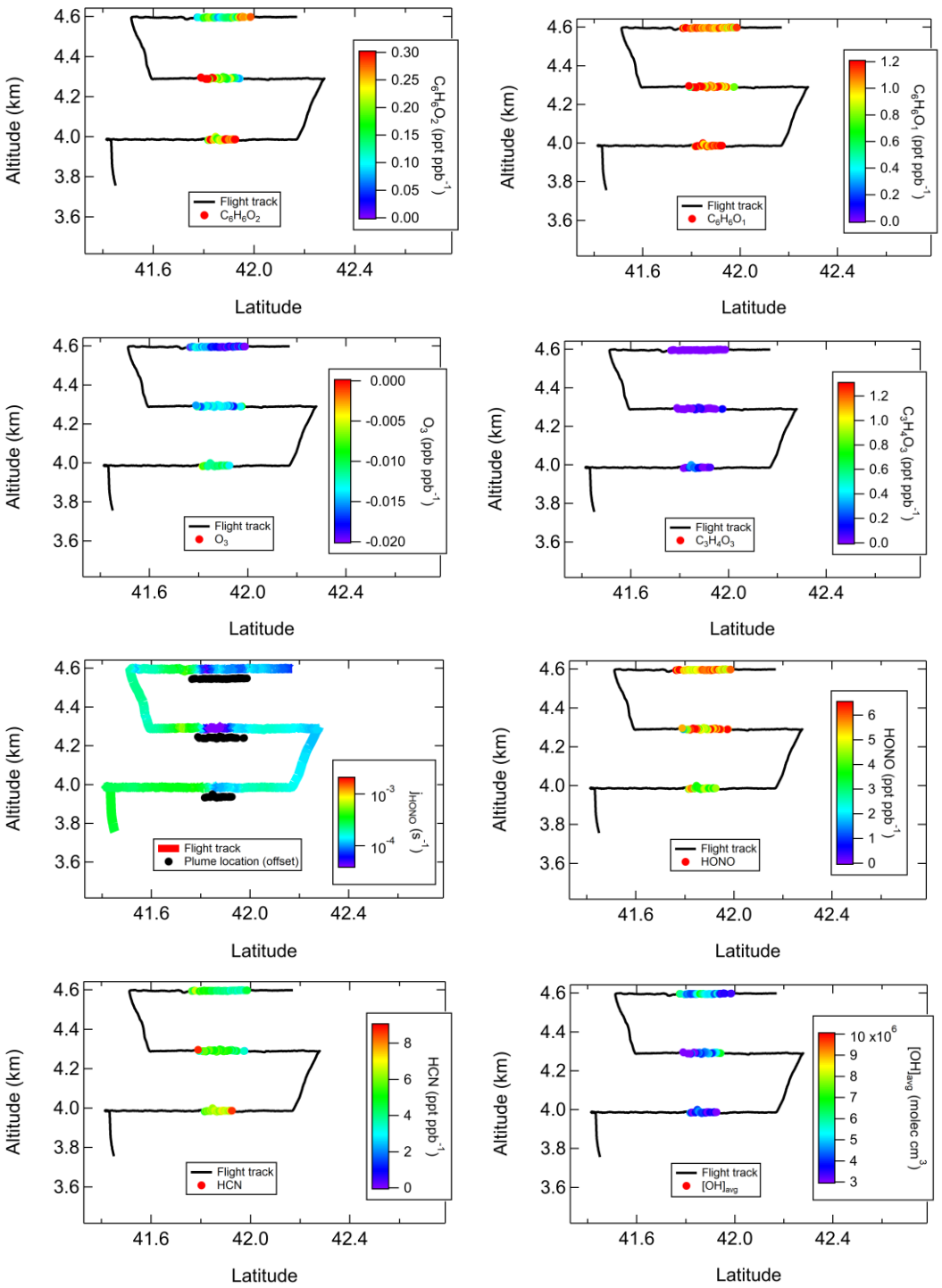

Figure S11. Various measurements in three vertically stacked transects at an estimated physical age of 47 min, sampled from 1850-1925 LT, close to sunset. O_3 is depleted relative to the background. HONO and $C_6H_6O_2$ remain in relatively high abundances across the plume transects, illustrating slower photochemistry leading to lesser gradients. This figure can be compared with Fig. S10, which shows a similar estimated physical age but sampled in the middle of daytime with more rapid chemistry and stronger gradients.

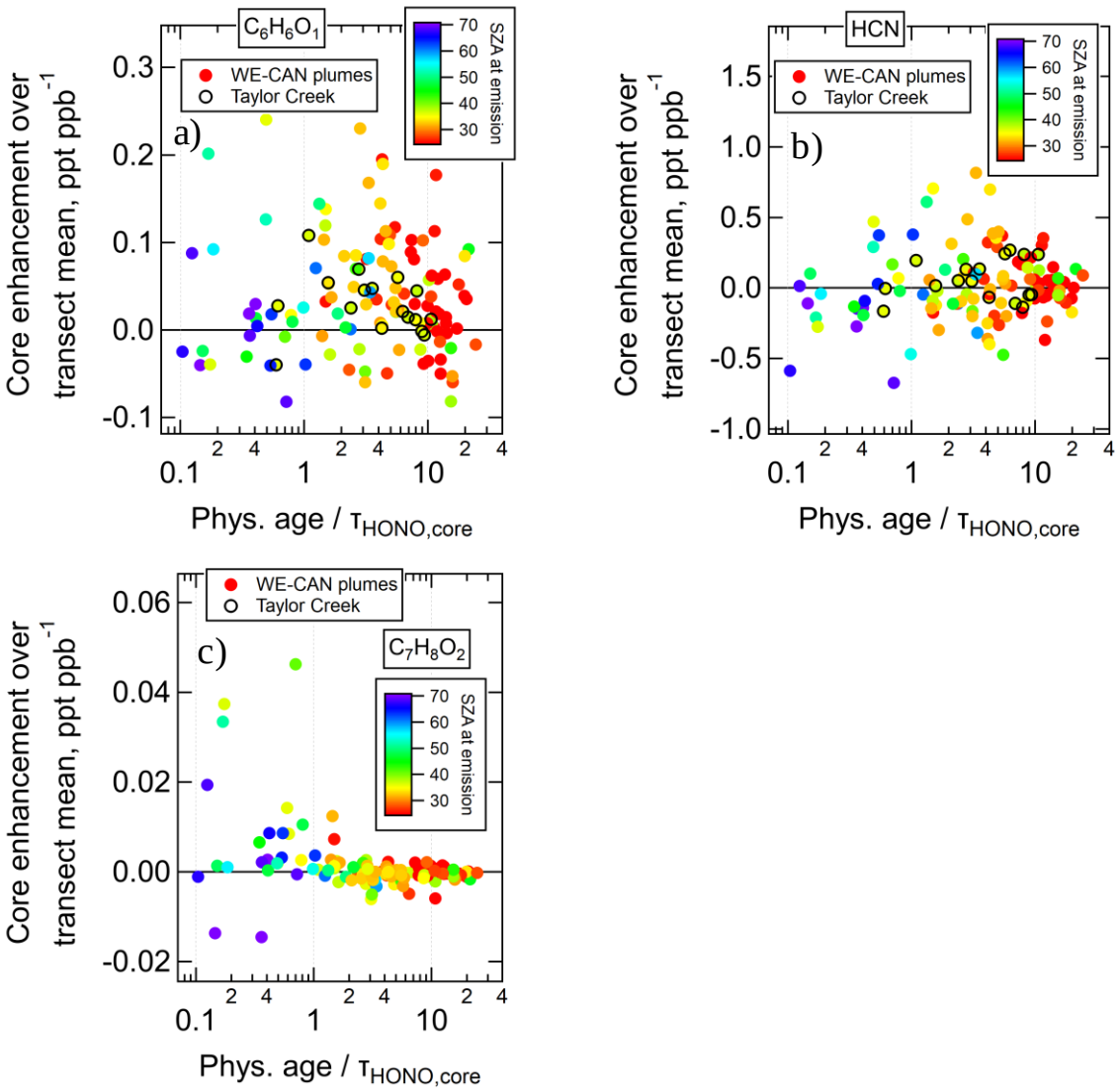

Figure S12. Enhancements of NEMRs in plume cores (average where [CO] > 90th percentile) relative to transect mean NEMRs for all WE-CAN transects, for a) $C_6H_6O_1$, b) HCN, and c) $C_7H_8O_2$ (methyl catechol; see Palm et al., 2020) for comparison with Fig. 4. The Taylor Creek plume transects are highlighted.

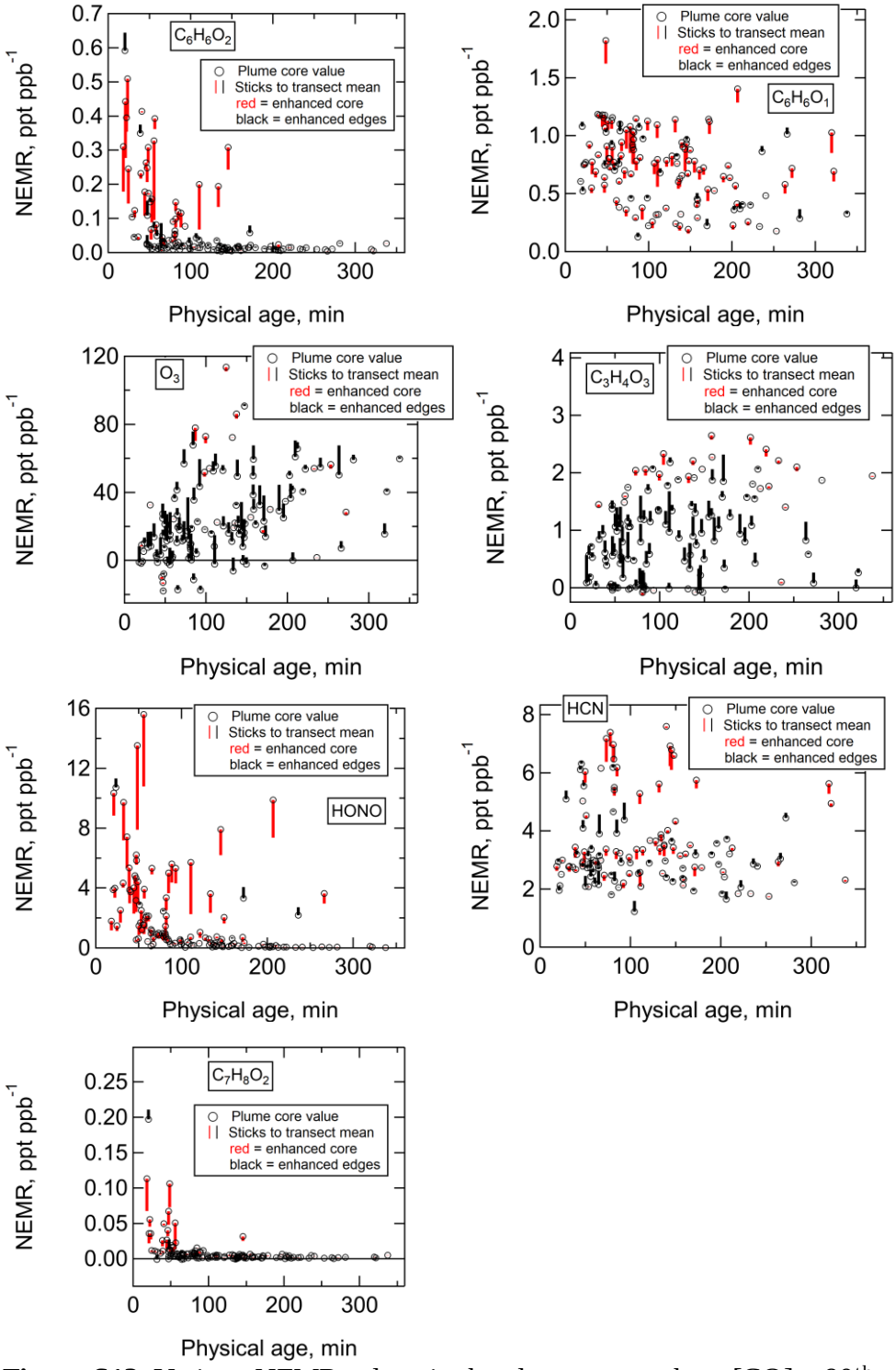

Figure S13. Various NEMR values in the plume cores where [CO] > 90th percentile (open circles), relative to transect mean NEMRs (other end of sticks). Sticks are red when the core is higher than the transect mean, and black when the core value is lower. Reactive emissions are generally enhanced in the core, oxidation products are enhanced on the edges, and unreactive compounds such as HCN show little gradients.

Table S1. Rate constants for reactions of OH with various compounds used in this analysis.

Molecular formula	Compound	k_{OH} rate constant (cm^3 $molecule^{-1}$ s^{-1})
$C_6H_6O_1$	Phenol	2.6×10^{-11} ([1])
$C_6H_6O_2$	Catechol	1.0×10^{-10} ([2])
C_7H_8	Toluene	5.6×10^{-12} ([3])
C_6H_6	Benzene	1.2×10^{-12} ([3])
CO	Carbon monoxide	2.4×10^{-13} ([4])

[1](Atkinson et al., 1989)
[2](Olariu et al., 2000)
[3](Atkinson & Arey, 2003)
[4](Burkholder et al., 2019)